**ORIGINAL CONTRIBUTION**

# Regional analysis of inflammation and contractile function in reperfused acute myocardial infarction by in vivo $^{19}$F cardiovascular magnetic resonance in pigs

Florian Bönner[1] · M. Gastl[1] · F. Nienhaus[1] · M. Rothe[2,3] · A. Jahn[1,4] · S. Pfeiler[1] · U. Gross[5] · H.-P. Schultheiss[5] · B. Ibanez[6,7,8] · S. Kozerke[9] · J. Szendroedi[10] · M. Roden[2,3,10] · R. Westenfeld[1] · J. Schrader[11,12] · U. Flögel[11,14] · G. Heusch[13] · M. Kelm[1,14]

## Abstract

Inflammatory cell infiltration is central to healing after acute myocardial infarction (AMI). The relation of regional inflammation to edema, infarct size (IS), microvascular obstruction (MVO), intramyocardial hemorrhage (IMH), and regional and global LV function is not clear. Here we noninvasively characterized regional inflammation and contractile function in reperfused AMI in pigs using fluorine ($^{19}$F) cardiovascular magnetic resonance (CMR). Adult anesthetized pigs underwent left anterior descending coronary artery instrumentation with either 90 min occlusion ($n = 17$) or without occlusion (sham, $n = 5$). After 3 days, in surviving animals a perfluorooctyl bromide nanoemulsion was infused intravenously to label monocytes/macrophages. At day 6, in vivo $^1$H-CMR was performed with cine, T2 and T2* weighted imaging, T2 and T1 mapping, perfusion and late gadolinium enhancement followed by $^{19}$F-CMR. Pigs were sacrificed for subsequent ex vivo scans and histology. Edema extent was $35 \pm 8\%$ and IS was $22 \pm 6\%$ of LV mass. Six of ten surviving AMI animals displayed both MVO and IMH ($3.3 \pm 1.6\%$ and $1.9 \pm 0.8\%$ of LV mass). The $^{19}$F signal, reflecting the presence and density of monocytes/macrophages, was consistently smaller than edema volume or IS and not apparent in remote areas. The $^{19}$F signal-to-noise ratio (SNR) > 8 in the infarct border zone was associated with impaired remote systolic wall thickening. A whole heart value of $^{19}$F integral ($^{19}$F SNR × milliliter) > 200 was related to initial LV remodeling independently of edema, IS, MVO, and IMH. Thus, $^{19}$F-CMR quantitatively characterizes regional inflammation after AMI and its relation to edema, IS, MVO, IMH and regional and global LV function and remodeling.

**Keywords** Cardiovascular magnetic resonance · Inflammation · Large animal models · Monocytes/macrophages · Myocardial infarction

## Introduction

Acute myocardial infarction (AMI) and ischemic heart disease remain the leading causes of death and heart failure [43]. All-cause mortality and rehospitalization for heart failure within 1 year after AMI are critically dependent on infarct size (IS)

[36]. Microvascular obstruction (MVO) and intramyocardial hemorrhage (IMH), two major features of myocardial reperfusion injury [15, 16], are of additional value in the prediction of late adverse regional and global left ventricular (LV) remodeling and mortality [6, 25, 29]. The processes of evolving edema, infarction, MVO, and IMH in reperfused AMI are dynamic and interact with inflammatory infiltration and the initiation of healing and repair [9, 19]; the repair relies on immune cell recruitment, most importantly monocytes and derived macrophages [37]. Monocytes/macrophages are attracted to the infarcted myocardium in a time- and region-dependent manner, as evidenced by histology in human myocardium [42]. Whereas inflammation is necessary for healing and repair, excessive inflammation is detrimental [14], and therapeutic modulation of inflammation after AMI might

✉ Florian Bönner
Florian.Boenner@med.uni-duesseldorf.de

Extended author information available on the last page of the article

reduce patient morbidity and mortality [12, 38]. Multiparametric [1]H-based cardiovascular magnetic resonance ([1]H-CMR) has become the gold standard for the noninvasive assessment of IS, MVO, IMH, and LV function after AMI [19]. However, there is an unmet need to visualize and quantify the spatial and temporal cellular inflammatory patterns in vivo.

Using experimental high-field (9.4 T) CMR, we established fluorine (^{19}F)-CMR to monitor monocytes/macrophages in mouse models [10]. [19]F MRI noninvasively monitors specifically infiltrating monocytes due to their rapid and specific uptake of intravenously applied perfluorocarbon nanoemulsions [3, 26]. Recently, we have demonstrated the technical feasibility of this ^{19}F-CMR approach also in clinical scanners (i.e. field strength of 3 T) [4, 33]. In the present study, we adapted this approach to a pig model of reperfused AMI which permits a spatially resolved regional analysis of inflammatory infiltration and its relation to edema, IS, MVO, IMH as well its impact on regional and global LV contractile function.

## Material and methods

### Reperfused acute myocardial infarction in pigs

Experiments were performed in 22 adult female Aachen minipigs [27] with a mean body weight of $67 \pm 9$ kg, in accordance with the national guidelines on animal care and approval by the 'Landesamt für Natur, Umwelt- und Verbraucherschutz' (L84-02.04.2013.A437 and L84-02.04.2016.A322). The experimental protocol is displayed in Fig. 1. Myocardial infarction was induced in pentobarbital-isoflurane-anesthetized closed-chest pigs by 90 min of pressure-wire-controlled left anterior descending (LAD) coronary artery occlusion [33], for details see supplemental material & methods and supplemental Figure I. In 5 sham animals the LAD was instrumented but not subjected to balloon occlusion.

### Production, quality control and application of perfluorooctyl bromide nanoemulsion

The perfluorooctyl bromide nanoemulsion (PFOB) was produced according to established protocols [4, 33]. A detailed description of the production, quality control, stability assessment, blood kinetics and phagocytosis of PFOB is provided in the supplemental Figures II and III. PFOB was infused intravenously on day 3 after AMI with 5 ml/kg body weight and a rate of 80 ml/h (Fig. 1) in all surviving animals ($n = 10$ AMI and $n = 5$ sham) according to previous protocols [4].

## [1]H and ^{19}F cardiovascular magnetic resonance data acquisition and histology

After proof of LAD patency 6 days after AMI by invasive angiography, CMR was performed using a whole-body 3.0-T Achieva X-series MR scanner (Philips Healthcare, Best, the Netherlands). In vivo CMR was performed according to previously established workflows and protocols for local signal precision with optimized ^{19}F sequences [33]. The ^{1}H and ^{19}F-sequence protocols and details are reported in supplemental Table I. After in vivo [1]H- and ^{19}F-CMR acquisitions, the pigs were euthanized inside the scanner for in situ imaging with arrested hearts. Autopsy was performed, and organs (heart, liver, spleen and sternum) were explanted and stored in 4% paraformaldehyde (PFA) for analysis of histopathology and distribution of PFOB with high resolution ^{19}F-CMR. A detailed description of the histopathological protocols and analysis, including the immunohistochemistry of TNFα, is provided in the supplemental material & methods and supplemental figure IV and V.

## Cardiovascular magnetic resonance data analysis

Dedicated software (Circle CVI 42, Circle Cardiovascular Imaging Inc., Calgary, AB, Canada) was used for full automatic delineation of ventricular contours, automatic calculation of volumes and analysis of parametric T1 and T2 maps. Due to misalignment of the automated contouring algorithm, significant manual correction of endocardial contours was necessary in 3/10 pigs after AMI. As described in detail in supplemental material & methods and shown in supplemental figure VI, volumes were indexed to body weight to measure end diastolic volume index (EDVi), end systolic volume index (ESVi), stroke volume index (SVi), cardiac index (CI) as well as ejection fraction (EF), global longitudinal strain (GLS), and early longitudinal diastolic strain rate (SRe) [34]. The sphericity volume index (ShVi) was calculated with EDV/ $((\pi/6) * L)^3$ [1]. Initial remodeling was defined as > 20% EDVi increase compared to the EDVi of sham-instrumented animals, adapted from studies investigating long-term remodeling after AMI [41]. T2 weighted images and T2 maps were analyzed for the extent of myocardial edema and expressed as % of LV mass or in absolute mass (g). T2* weighted images were analyzed for IMH and expressed as % of LV mass or in milliliters (ml). Contrast-enhanced images were analyzed at first pass for myocardial perfusion and late gadolinium enhancement (LGE) after 10 min for IS (> 5 SD threshold), border zone (BZ) (> 2 < 5 SD threshold) [20] and after 15 min for MVO and expressed as % of LV mass or in milliliters
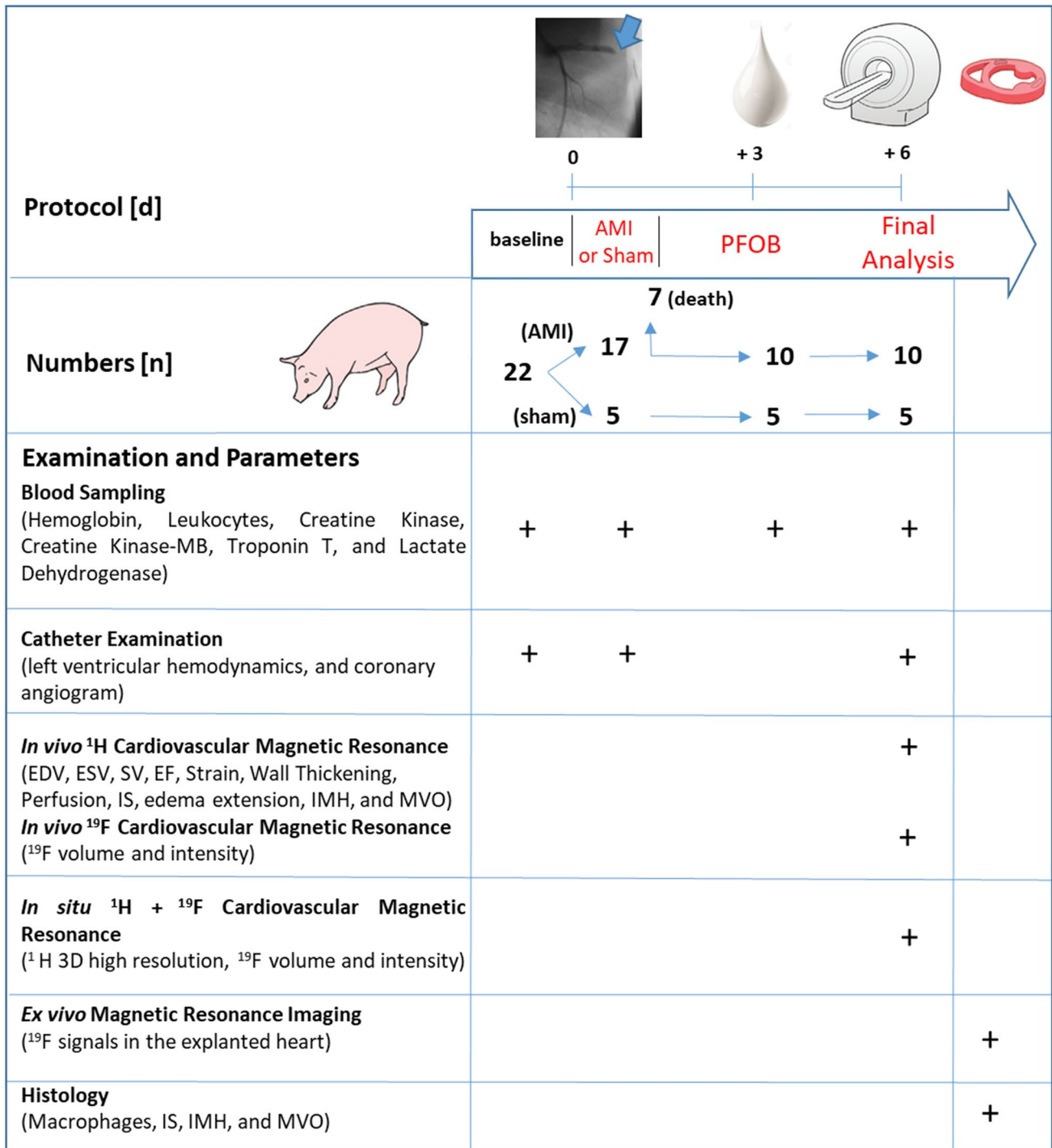
**Fig. 1** Study design and protocol. Seventeen pigs were subjected to acute myocardial infarction (AMI), and 5 pigs underwent sham surgery. A perfluorooctyl bromide (PFOB) nanoemulsion was administered on day 3 after AMI. Fifteen pigs underwent in vivo cardiovascular magnetic resonance (CMR + $^{19}$F) with analysis of volumes, contractile function and tissue characterization. In situ and ex vivo magnetic resonance imaging, followed by histology, was performed for validation purposes. *EDV* end diastolic volume, *ESV* end systolic volume, *SV* stroke volume, *EF* ejection fraction, *IS* infarct size, *IMH* intramyocardial hemorrhage, *MVO* microvascular obstruction

(ml) [34]. Volumes containing $^{19}$F signals were quantified using the 3D visualization software Amira 4.0 (ThermoFisher Scientific,Waltham,USA), and image fusion of $^{1}$H/$^{19}$F-datasets was performed with HOROS (Nimble Co LLC,USA). The fused images of all 10 animals which were included in the final analysis are shown in the supplemental

figure VII. For quantification of $^{19}$F-signals, the primary signal in a respective region was corrected according to the coil sensitivity profile as outlined in supplemental figure VIII. The signal-to-noise-ratio (SNR) of respective regions was calculated from the ratio of the signal intensity mean of a region-of-interest (ROI) and the standard deviation of a background-noise ROI in the same slice located out of the thorax at comparable coil distance. $^{19}$F volumes were calculated by applying background subtraction with SNR 7, which was sufficient to subtract all unspecific technical background signals (outside the body). The $^{19}$F-integral was the product of SNR and volume.

## Statistical analysis

Statistical analysis was performed using SPSS software (version 24.0, IBM, Armonk, NY, US). Unless otherwise stated, continuous variables are presented as the mean ± standard deviation (SD). Differences between the two groups (sham and AMI) were analyzed by Student's 2-sided unpaired $t$ test for normally distributed data and Mann–Whitney $U$ test for non-normally distributed data. Pearson's or Spearman's correlation were used to assess the relationships between different CMR parameters. Separate linear regression models in pairwise combination with edema, IS, MVO, and IMH were created to adjust the univariate correlations of $^{19}$F with LV function and volumes for these parameters to test whether $^{19}$F would independently predict LV function and geometry. ROC analysis was used to identify optimal cut-off values for prediction of initial remodeling ($> 20\%$ EDVi increase compared to the sham animals mean) (AUC 0.87) or impaired remote systolic wall thickening ($<$ cohort median of diastolic wall thickening) (AUC 0.78). The respective $p$ values are reported in the figures.

## Results

### Acute myocardial infarction and safety of perfluorooctyl bromide nanoemulsion

Twenty-two pigs were included in the study. Baseline and procedural characteristics of sham pigs ($n = 5$), AMI survivors ($n = 10$) and AMI non-survivors ($n = 7$) are reported in supplemental Tables II and III. There were no differences in baseline characteristics between survivors and non-survivors. The cause of death ($n = 7$) was ventricular fibrillation refractory to defibrillation in all pigs. No pig died beyond 90 min of ischemia. There was no serious adverse side reaction when pigs received PFOB on day 3 after AMI (supplemental Table IV). The blood kinetics of PFOB are given in supplemental Figure III and revealed an almost complete clearance from the circulation 3 days after injection. Ten

pigs had a patent LAD on day 6 after AMI on coronary angiography and were included in the CMR study.

### LV function and initial remodeling early after AMI

Edema extent was $35 \pm 8\%$ of LV mass and IS was $22 \pm 6\%$ of LV mass. Six of 10 surviving pigs had MVO ($3.3 \pm 1.6\%$ of LV mass), and the same animals also had IMH ($1.9 \pm 0.8\%$ of LV mass). Figure 2 shows systemic hemodynamic, volumetric and functional data 6 days after AMI. Compared to sham pigs, pigs with AMI had a slight increase in heart rate, a trend toward lower arterial pressure and higher systemic vascular resistance. SVi, CO, EF and LGE were reduced; ESVi, EDVi and ShVi were increased. Thus, the present model provided robust infarction with early LV dysfunction and initial remodeling of varying inter-individual severity.

### $^{19}$F monocyte/macrophage signals co-register with the infarct area

The average acquisition time of the 3D-whole heart $^{19}$F-information was $18 \pm 2$ min. Figure 3 displays the correlation of local $^{19}$F-signal intensity and monocyte/macrophage density. $^{19}$F-signals were restricted to infarcted tissue and its border zone, as delineated by infarct size imaging with LGE, while remote myocardial areas displayed no $^{19}$F-signal (Fig. 3A, left). The colocalization of the $^{19}$F-label with monocytes/macrophages was confirmed by histology (Fig. 3A, right and B). The infarct area displayed patchy infiltration with monocytes/macrophages, mirrored by the respective local $^{19}$F signals. An equal number of M1 (CD68$^{high}$ CD163 $^{low}$) and M2 (CD68$^{low}$ CD163$^{high}$) macrophages was present within the areas of $^{19}$F signal (supplemental Figure V). The mean $^{19}$F-signal intensity was quantified considering the coil sensitivity profile (supplemental Figure VIII) and expressed as myocardial $^{19}$F-SNR. The calculated local mean $^{19}$F SNR acquired in vivo correlated with the mean monocyte/macrophage density determined by histology (Fig. 3C; $R^2 = 0.6075$, $p < 0.0001$). The individual localization of the analyzed regions of interest is given in the supplemental Table V. The $^{19}$F detection threshold was 70,000 cells/mm$^3$. In sham pigs, no myocardial $^{19}$F signal was observed, and immunohistochemistry did not show signs of acute myocardial inflammation.

Figure 4 shows the individual whole heart quantitative $^{19}$F-analysis of all surviving pigs. For inter-individual image comparison, $^{19}$F-signals of all 10 pigs are shown in supplemental Figure VII. The monocyte-dependent $^{19}$F-signals were also observed in the bone marrow of the sternum and ribs (Fig. 4A and supplemental Figure IX). These signals could easily be distinguished from AMI signals and did not disturb the signal quality or quantification. After cardiac segmentation, the average volume covered by $^{19}$F-signals per heart was
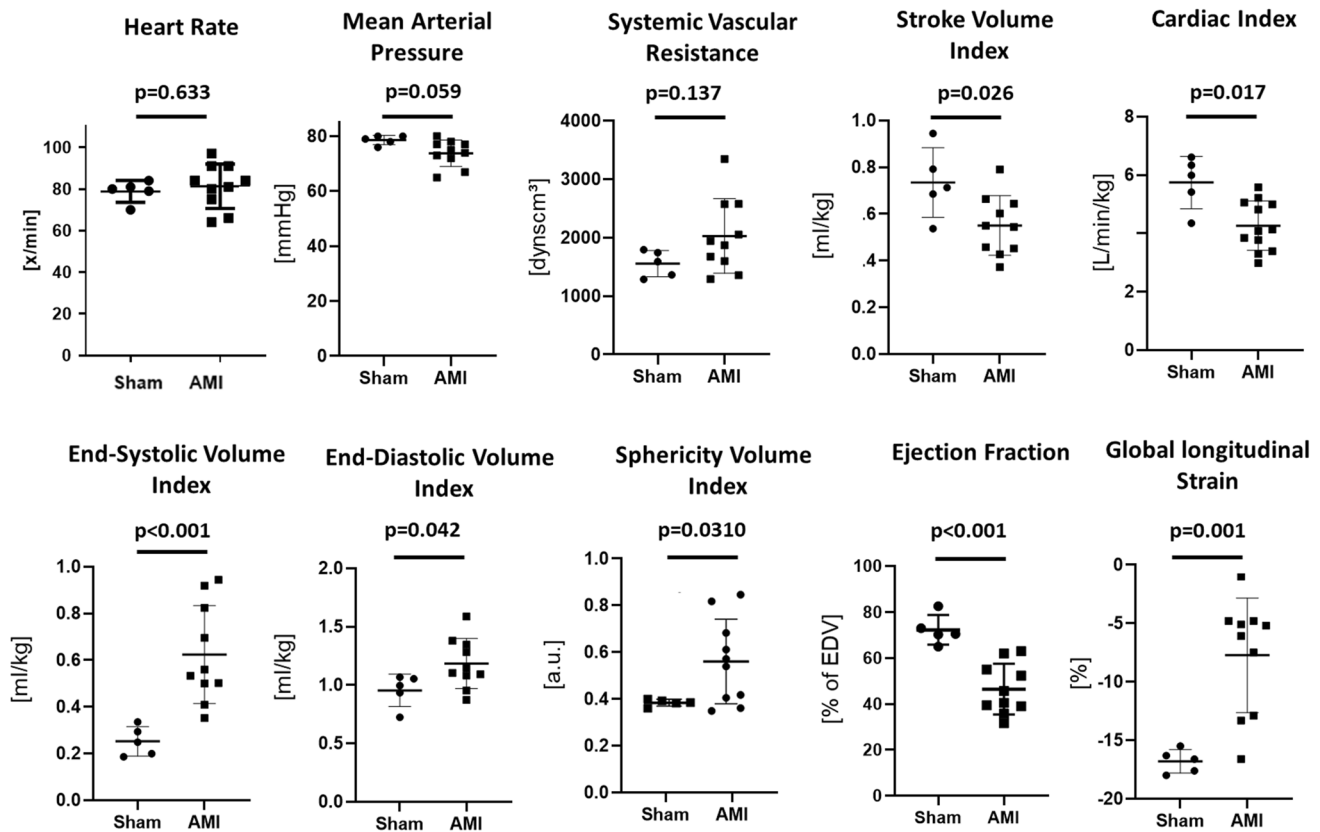
**Fig. 2** Systemic hemodynamics, left ventricular contractile function and volumes. Quantitative analysis of hemodynamic parameters 6 days after acute myocardial infarction (AMI) compared to the sham procedure. Single values and the mean $\pm$ SD as well as the respective $p$ values calculated by unpaired Student's $t$ test are given

$15.8 \pm 9.5$ ml, and it was always within and smaller than the respective individual edema extent ($31.3 \pm 8.7$ ml) (Fig. 4A, B) and IS ($20.9 \pm 6.5$ ml) (Fig. 4A, C). The mean myocardial ^{19}F SNR was $13.3 \pm 4.7$ with a considerable inter-individual and segment-wise variation. As shown in Fig. 4D, there was a correlation of ^{19}F-SNR with ^{1}H derived T1 and T2 times taken from the infarcted segments of all pigs. Along with the systemic inflammatory response, we identified a correlation ($R^2 = 0.66$) of the individual increase in circulating leukocytes from baseline until day 3 and the ^{19}F integral (supplemental Figure III D).

## Segmental [19]F- and [1]H-CMR-derived infarct tissue characteristics

As shown in Fig. 5A + B, not all myocardial segments with edema and infarction were positive for the ^{19}F-CMR derived monocytes/macrophages signals. The correlation of edema extent and IS with the ^{19}F-integral was only fair. Pigs with high ^{19}F integral displayed only minor volume of MVO with concomitant IMH (Fig. 5 D + E). Apparently, the ^{19}F-CMR

derived monocytes/macrophages signal was of patchy nature with only fair correlation to edema extent or IS, and the ^{19}F integral was reduced in pigs with MVO and IMH. As shown in the supplemental figure X, hemorrhage itself had no impact on ^{19}F SNR.

## Association of border zone ^{19}F-signal with remote myocardial contractile function and initial ventricular remodeling

As shown in Fig. 6A, regional wall thickening displayed a gradient from infarct core to remote myocardium, while ^{19}F SNR decreased in most pigs from infarct core to remote myocardium. Interestingly, the ^{19}F-signal in the infarct border zone correlated inversely with the neighboring remote myocardial wall thickening (Fig. 6B). Histological analysis revealed significant TNF-$\alpha$ signals in remote cardiomyocytes of those pigs with high border zone ^{19}F SNR (6F + 6G). Increased ^{19}F-integrals over the entire heart correlated with enlarged EDVi and ShVi in univariate analysis. Even when adjusted for edema, IS, MVO and IMH, respectively,

**Fig. 3** Correlation of in vivo $^{19}$F signals to macrophage density in histology. **A** Left: $^{19}$F-signals are heterogeneously distributed in the area of infarction as observed in vivo (red lines) and ex vivo (white box). Right: infarct histology with Masson's trichrome strain: infarcted tissue = purple, granulation tissue = blue; fluorescent staining with anti-macrophage antibodies: CD68 (green, pseudocolored) and CD163 (red, pseudocolored) at ×40 magnification. Nuclear staining with DAPI (blue). Scale bar 7 mm at Masson's trichrome strain and 50 μm at fluorescence staining. **B** Segmental analysis with red ($^{19}$F) and black (macrophages) color intensity codes for the percentage of all individuals positive for the respective segment. **C** In vivo $^{19}$F SNR plotted against histological macrophage density expressed as cells/mm$^3$. Shown are data points of all animals. At least 5 regions of interest distributed in at least 2 different slices were considered per animal. If animals had $^{19}$F signal in more than 5 regions in at least 2 different slices due to their large $^{19}$F volume, those data points were additionally taken into consideration
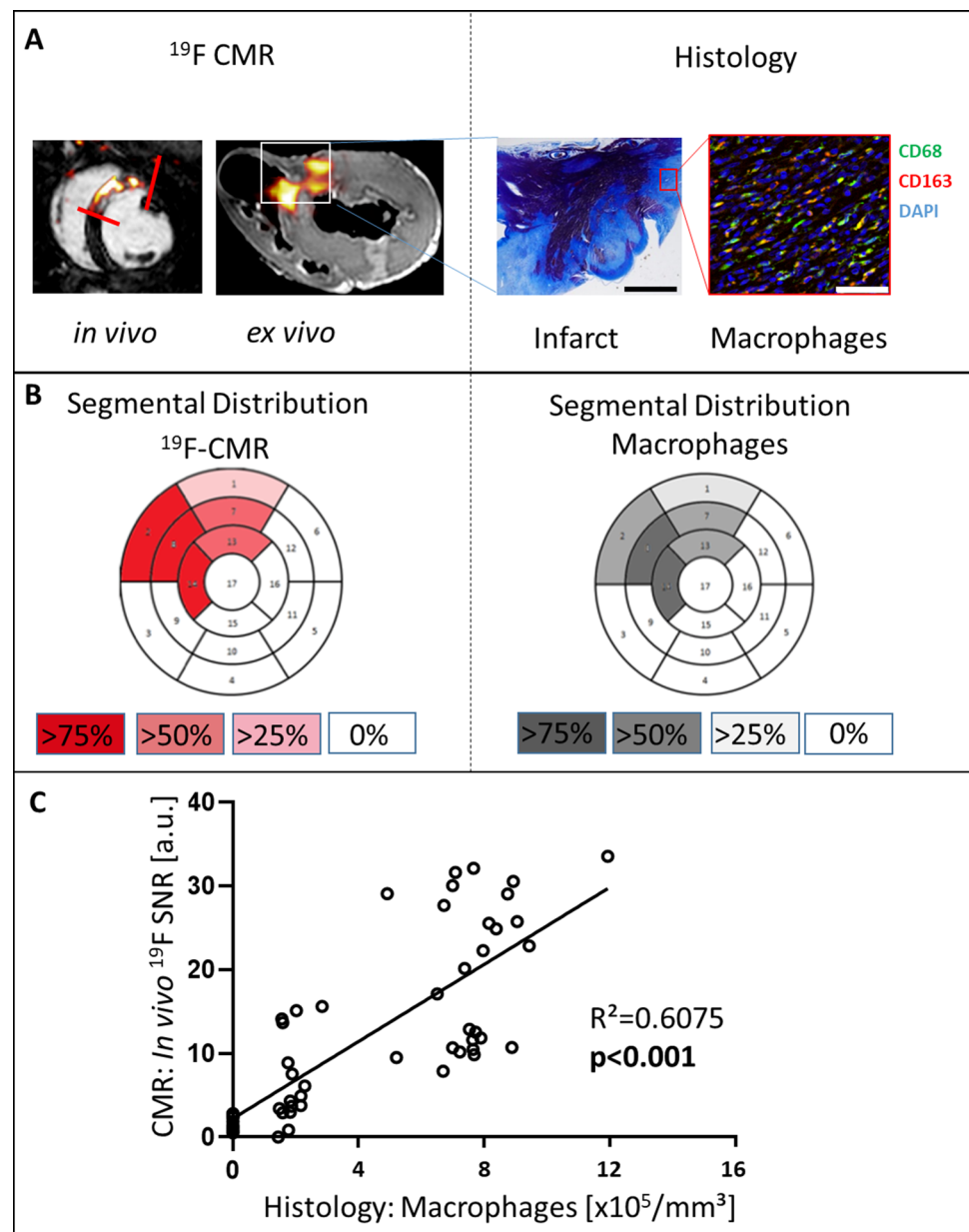


in multivariate models, the macrophage/monocyte derived $^{19}$F-signal was independently associated with initial LV remodeling (supplemental Table VI).

As demonstrated in Fig. 7, a cut-off $^{19}$F-integral value of 200 combined with a border zone SNR > 8 predicted impairment of remote myocardial contractile function and LV remodeling on day 6 after AMI. Pigs with whole heart $^{19}$F-integral > 200 and border zone SNR > 8 ($n = 5$) had less remote myocardial systolic wall thickening ($29.4 \pm 6$ vs. $59 \pm 16\%$, $p = 0.005$), larger EDVi ($1.4 \pm 0.1$ vs. $1.0 \pm 0.1$ ml/kg body weight, $p = 0.005$) and larger ShVi

($0.7 \pm 0.1$ vs. $0.4 \pm 0.1$, $p = 0.005$) than pigs with whole heart $^{19}$F-integral < 200 and border zone SNR < 8 ($n = 5$).

## Discussion

In the present study using a pig model of reperfused AMI, $^{19}$F-CMR noninvasively provided quantitative information about regional inflammatory infiltration of monocytes/ macrophages early after AMI and its association with LV contractile function and geometry. Inflammatory

**Fig. 4** $^{19}$F signals co-register with the infarct area. **A** $^1$H images with T2 mapping for identification of edema (blue lines) and late gadolinium enhancement (LGE) for infarct size (gray lines) were recorded (left) and fused with $^{19}$F images representing patchy macrophage presence (red lines). The $^{19}$F image overlay with the $^1$H image was performed automatically encoded with the "hot iron-lookup table" (HILT) in arbitrary units (right). Red arrows = signals in the sternum and ribs. Quantitative analysis of individual whole heart $^{19}$F volumes (HILT) and **B** edema extent (blue) as well as **C** infarct size (gray). **D** The $^{19}$F signal-to-noise ratio (SNR) of infarcted segments was significantly correlated with local T2 and T1 times.
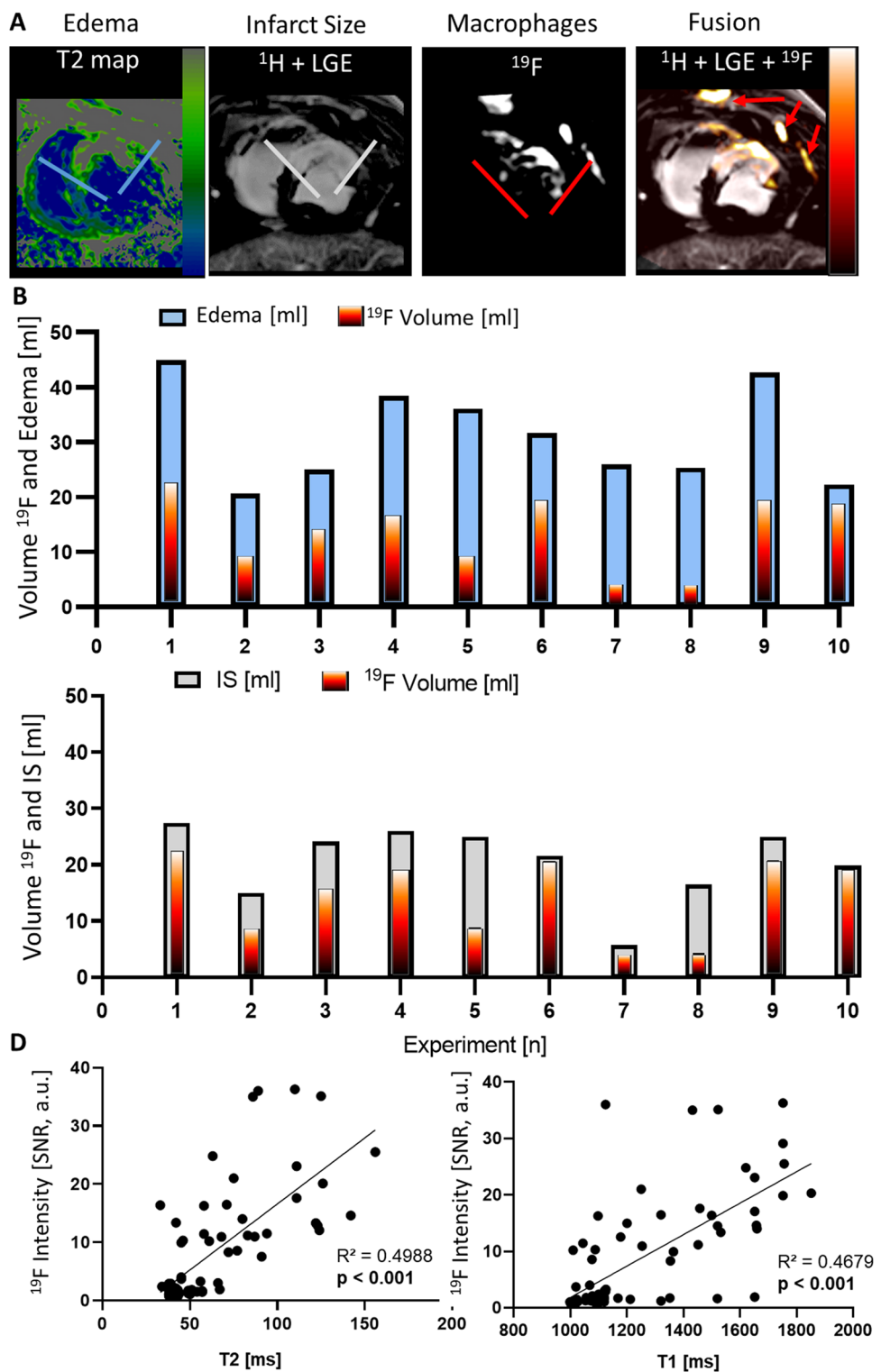


infiltration in the infarct border zone correlated with impaired remote myocardial systolic wall thickening and initial LV remodeling. The inflammatory signal over the entire heart correlated to impaired LV contractile function and remodeling independently of myocardial edema, IS, MVO, and IMH.

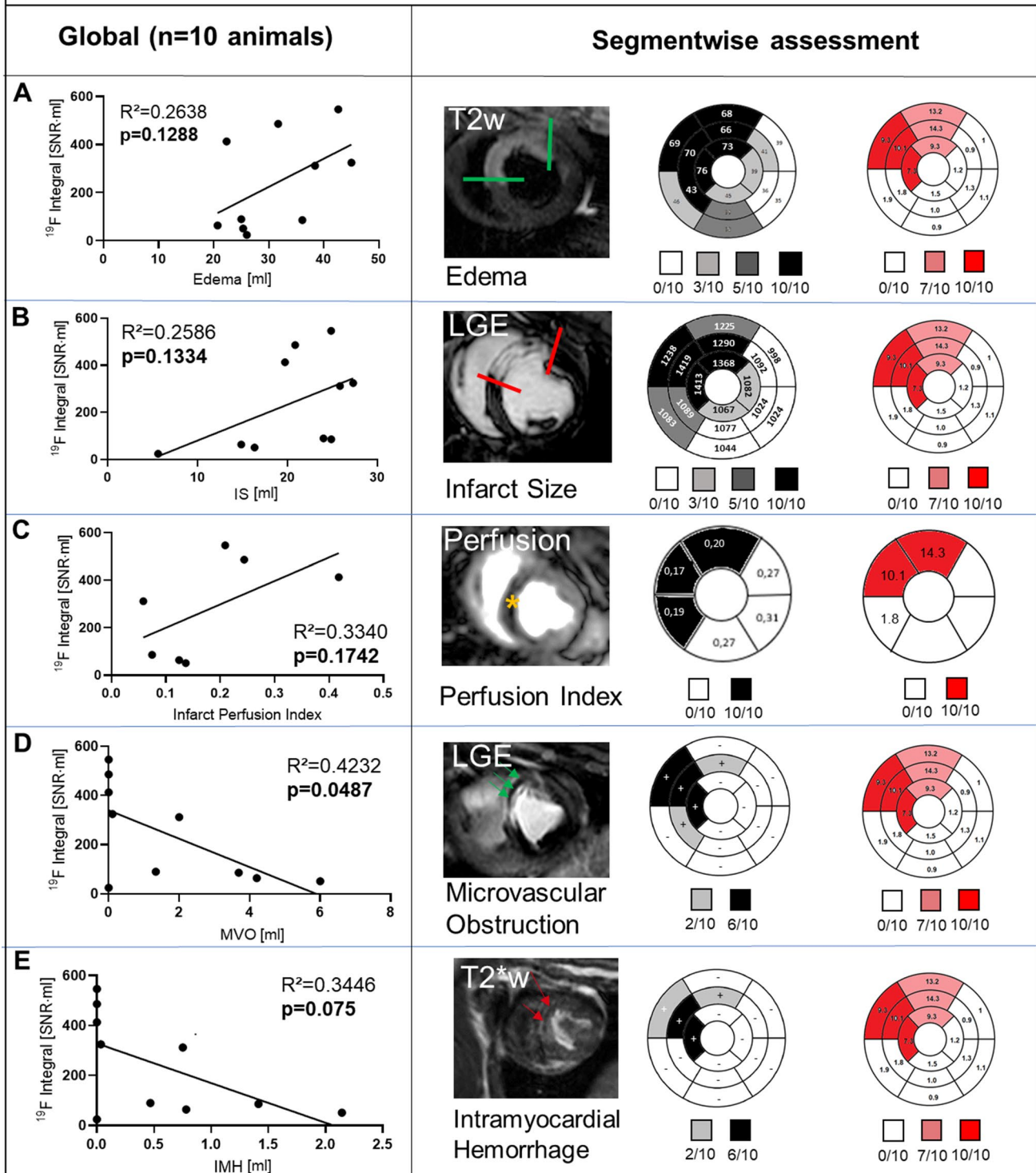$^{19}$F-CMR Inflammatory Infarct Core Pathology and $^{1}$H-CMR Infarct Tissue Markers

◄**Fig. 5** Segmental analysis of $^{19}$F integral and infarct tissue characteristics. Whole heart correlation of the $^{19}$F integral (Signal-to-noise-ratio [SNR] * ml) with infarct tissue characteristics (ml): **A** edema extent, **B** infarct size (IS), **C** regional perfusion, **D** microvascular obstruction (MVO) and **E** intramyocardial hemorrhage (IMH). The whole heart analysis, using a bivariate correlation model, revealed only MVO inversely correlated with $^{19}$F volume. Global and regional (segmental) analysis for the respective infarct pattern is given with example images (edema extent = green borders, IS = red borders, regional perfusion defect = yellow star, MVO = green arrows, IMH = red arrows). The bullseye plots are shown with color intensity coding according to the individuals positive for the respective segment. Additionally, $^{19}$F Signal to Noise Ratio, T1 and T2 values, as well as perfusion index, are given in mean values ($n = 10$ animals) per segment. IMH and MVO segments are indicated with "−"and "+"

## In vivo imaging of monocytes/macrophages with $^{19}$F-CMR

Our preliminary experiments were conducted to test and prove the applicability of various components and processes necessary for the planning, initiation and conduction of the present study. First, we tested optimal $^{19}$F containing nanoemulsions with respect to safety, dose and timing of the emulsion administration [4]. $^{19}$F measurements were done in explanted hearts to assure easy and sufficient $^{19}$F signal acquisition [4]. Thereafter, we tested and improved the in vivo CMR approach-applicability with $^{19}$F signal distance > factor 100 compared to explanted hearts and respiratory as well as cardiac movement [33]. After these experiments, it was clear, that a bFFE sequence with an off-set frequency of 58 ppm would be the best compromise for signal precision and SNR [33].

The findings of these preliminary studies (dose, timing, optimized sequences, work flows) were necessary to efficiently conduct the present study. The specific novelty of the present approach is the comparison of state-of-the-art CMR tissue markers as well as local and global myocardial function after AMI with the in vivo $^{19}$F signal, which was also validated by histology.

Since $^{19}$F-CMR is essentially background-free, perfluorocarbon nanoemulsions are the primary source of the $^{19}$F-signal, and they are preferentially taken up by monocytes/macrophages [3, 26]. In the present study, the nanoemulsion was administered on day 3 after AMI to allow for sufficient uptake into monocytes/macrophages [26] and to induce a maximum monocyte/macrophage signal in the injured myocardium on day 6 after the insult. Untargeted perfluorocarbon nanoemulsions are taken up by M1 and M2 tissue macrophages to an equal extent [13]. Since both cell types were present in equal numbers in our study on day 6 after reperfused AMI, the $^{19}$F-signal observed reflected most likely a mixture of a M1 and a M2 macrophage infiltration. Additionally, the $^{19}$F-signal was closely associated with altered tissue relaxation properties indicating early tissue

reorganization in infarcted myocardium with a high volume and density of monocytes/macrophages.

As an alternative to $^{19}$F labeling of immune cells, ultrasmall iron oxide nanoparticles (USPIOs) enhanced $^1$H-based CMR has been used. USPIOs also preferentially label monocytes/macrophages and significantly affect $^1$H relaxation properties. This technique, leading to signal voids in the area of monocytes/macrophages, has provided initial, promising diagnostic results in patients after AMI, but its specificity has been hampered by interference with IMH [29, 46]. Beyond direct visualization of immune cells, the metabolic signature of inflammation can be assessed with positron-emission tomography (PET) or hyperpolarized CMR [23, 24, 31, 32].

PET MRI using 18F-fluorodeoxyglucose (18F-FDG) has proven significant value in the detection of atherosclerosis-related inflammation and in predicting restenosis in peripheral artery disease [5, 8]. There are specific nuclear PET tracers for imaging monocytes/macrophages after AMI [30, 31, 39]. Indeed, combined PET-MRI approaches have identified certain cell types and inflammatory activity using optimized image resolutions of $4 \times 4 \times 4$ mm$^3$ [8]. However, a direct quantification of the signal in terms of local cell abundance is difficult due to tracer/image acquisition timing and complex post-processed image reconstructions. The need for cost intensive specialized equipment (linear accelerator) and staff (chemist) might hamper the applicability of PET/MRI in clinical routine. The $^{19}$F principle easily works on the widely available CMR platform, with an image resolution $(1.35 \times 1.35.1.5$ mm$^3)$ sufficient for imaging inflammatory foci in the AMI border zone with a directly quantifiable signal, without the need for additional specialized equipment and personnel.

With the present CMR approach, the images of monocyte/macrophage infiltration were generated in vivo with a resolution and acquisition time comparable to clinical standard sequences and protocols (supplemental Table I). The pig model of reperfused AMI in the present study exhibited a similar extent of IS and frequency of MVO or IMH as typical patients with an anterior STEMI [6, 29]. Moreover, the monocyte/macrophage density was comparable to histopathological studies in patients [42], rendering the present model suitable for translational perspectives. Thus, $^{19}$F-CMR is a highly promising imaging technique for clinical trials aiming to further evaluate the effects on monocyte/macrophage infiltration in patients early after AMI.

## Inflammatory infiltration and remote myocardial contractile function and initial left ventricular remodeling

In vivo myocardial $^{19}$F-signals revealed not only considerable inter-individual variation, which correlated to

**Fig. 6** The border Zone $^{19}$F signal is associated with impaired remote systolic wall thickening and the whole heart $^{19}$F integral with initial remodeling post-AMI. **A** Myocardial systolic wall thickening (% of end diastolic thickness, gray) and $^{19}$F signal-to-noise ratio (SNR, orange) of the infarct core (IC), border zone (BZ) and remote myocardium (RM). **B** Correlation of RM systolic wall thickening to BZ $^{19}$F SNR. (C) $^{19}$F signal distribution across IC, BZ and RM as delineated by $^{1}$H magnetic resonance imaging with late gadolinium enhancement (LGE), **D** schematic assignment of left ventricular territories with region-of-interest pointing towards **E** representative histological (Hematoxylin Eosin Stain) overview of IC, BZ and RM. Scale bar 2.5 mm. **F** Histology of BZ/RM at identical region-of-interest with staining for macrophages (CD68, green) and TNF-α (red); Scale bar 50 µm. The blue line is highlighting the border of structurally intact cardiomyocytes as delineated by autofluorescence. Within BZ, there is a clear overlap of TNF-α+spots with CD68+spots. In RM, blue arrows point towards TNF-α spots within cardiomyocytes as delineated by their autofluorescence. Correlation of whole heart $^{19}$F integral with end diastolic volume index (**G**) and sphericity volume index (**H**)
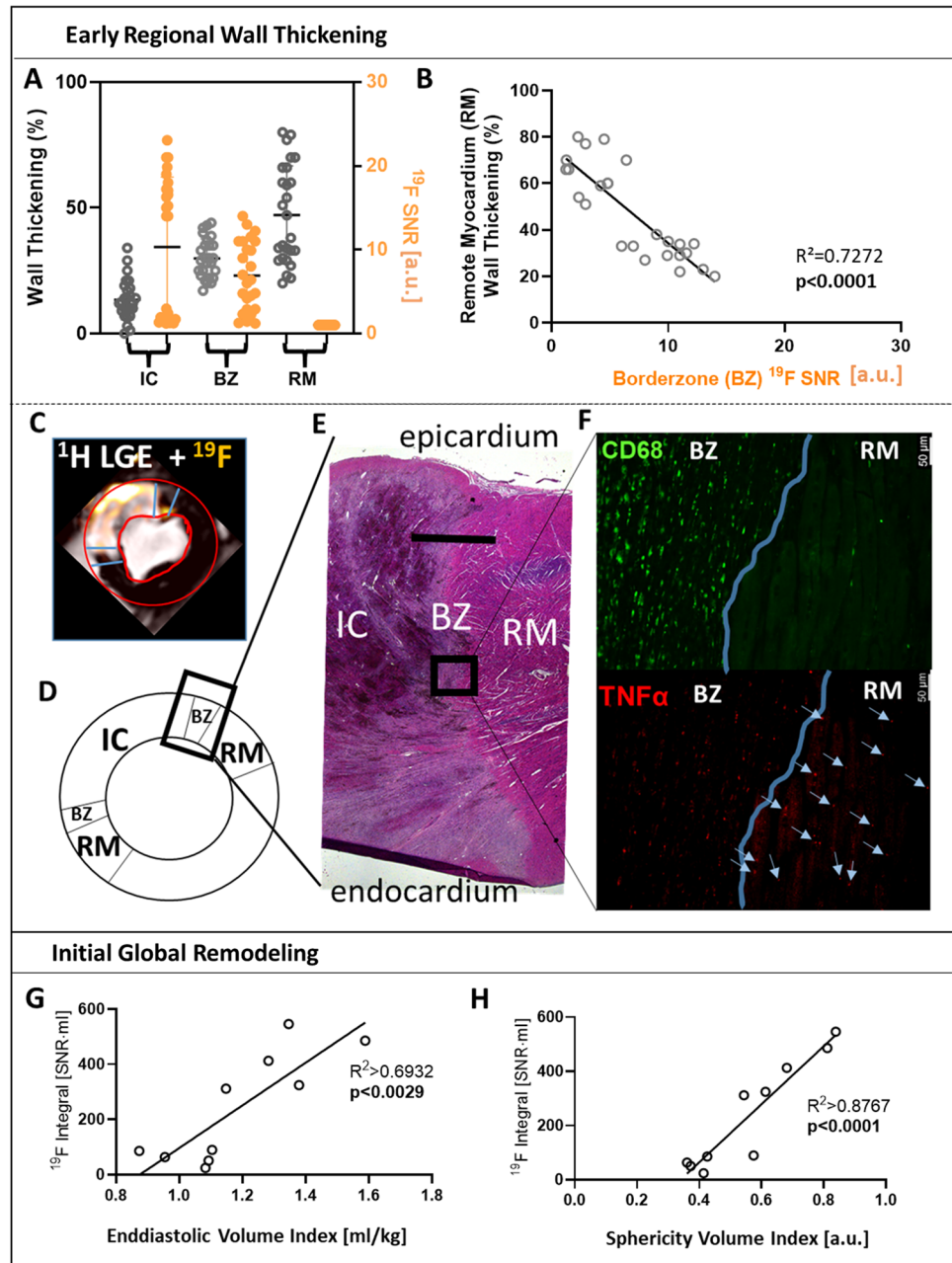


the systemic increase in leukocytes (supplemental figure IIID), but also a patchy appearance in myocardial infarction, which was validated by histology (Fig. 3). The spatial heterogeneity of monocytes/macrophage infiltration was reflected in features of the $^{19}$F-signal: Even those pigs with low $^{19}$F whole heart volumes (< 5 ml) had a mean myocardial $^{19}$F-SNR of > 10, indicating hot spots of monocyte/macrophage infiltration as known also from human autopsy studies [42]. The area of myocardial edema and IS was not entirely invaded by monocytes/macrophages as evidenced by $^{19}$F-CMR. Moreover, the incidence of MVO and IMH was even reduced in segments positive for $^{19}$F-CMR. Since

MVO and IMH coincided in our model (day 6 after AMI), in good agreement to clinical observations [29], the attenuating effect of MVO on monocyte/magrophage infiltration, which has already been shown by other groups [45], might have counterbalanced the pro-inflammatory effect of IMH at day 6 [2].

Our present study provided novel information on the regional relationship between monocyte/macrophage infiltration in the infarct border zone with systolic wall thickening in the adjacent remote viable myocardium (Fig. 6A + B) and with LV remodeling early after AMI (Fig. 6G + H). The infarct border zone derived $^{19}$F-signal correlated

**Fig. 7** $^{19}$F signaling provides additional information on initial remodeling and remote myocardial contractile function early after myocardial infarction. At comparable infarct sizes and areas at risk, increased macrophage signals delineated by $^{19}$F-CMR are associated with impaired remote myocardial contractile function and remodeling early after AMI. Representative images of two pigs after stratification for the whole heart $^{19}$F integral >/< 200 SNR × ml and border zone $^{19}$F SNR >/< 8 are shown. The edema extent (blue borders) and infarct size (green borders) were comparable. Images of LV areas in end diastole and end systole display differences in remote myocardial contractile function and ventricular shape. The $^{19}$F cut-off identifies pigs with impaired remote wall thickening and larger end diastolic volume index (EDVi).
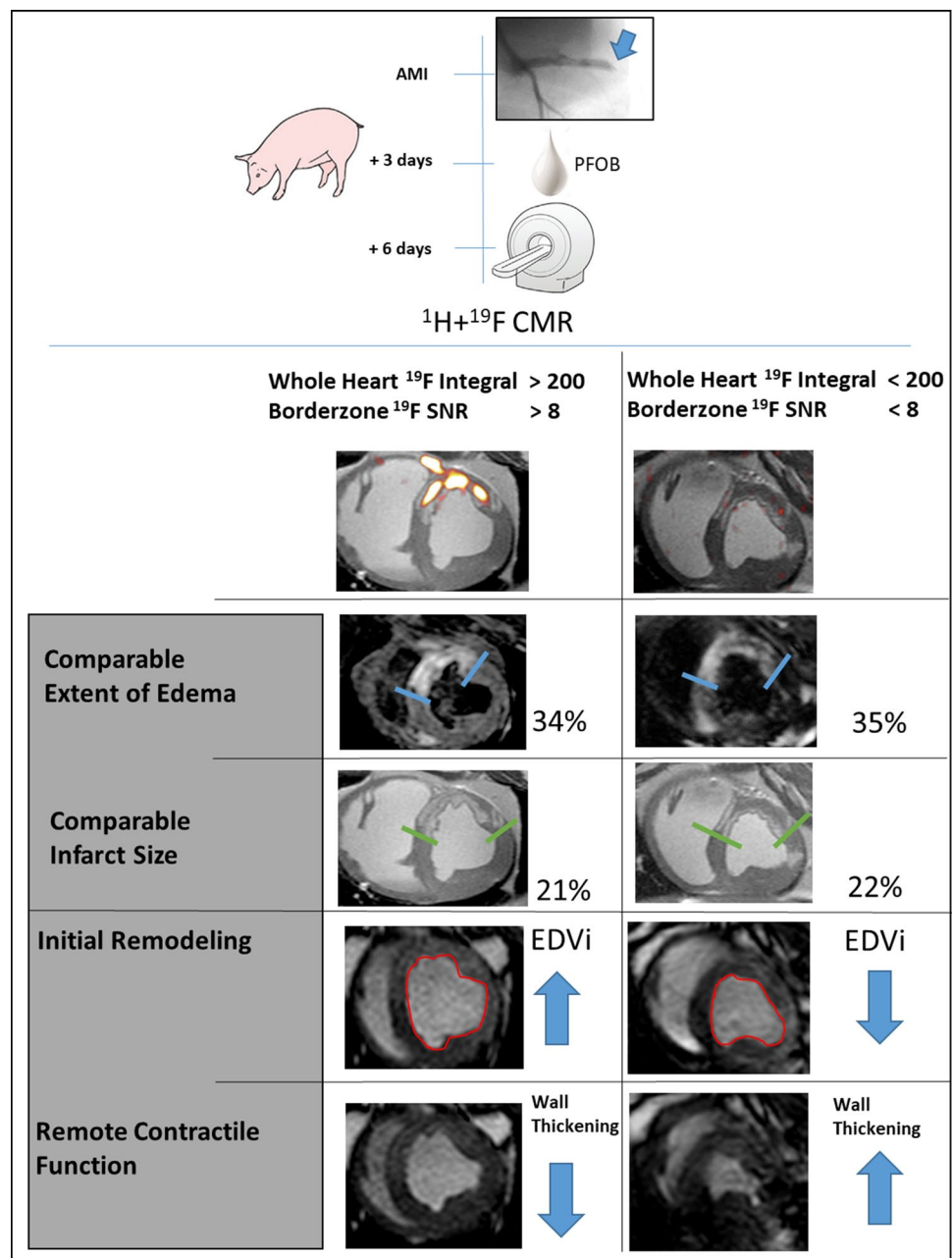


inversely with remote myocardial systolic wall thickening. On histology, TNF-α was identified in remote cardiomyocytes (Fig. 6F). A spillover of cytokines with a negative inotropic action such as TNF-α from the border zone into the remote myocardium might thus explain the impaired wall thickening possibly mimicking stunned myocardium [17]. It is unclear to what extent such increased TNF-α levels are derived from monocytes/macrophages or the cardiomyocytes in the inflamed border zone, as shown in microembolized myocardium [7, 18].

On the level of a global analysis over the entire heart, the global $^{19}$F integral was associated with LV remodeling on univariate analysis. In multivariate analysis, the correlation of the global $^{19}$F integral was independent from edema, IS, MVO, and IMH, respectively. The greater the monocytes/macrophages infiltration, as indicated by $^{19}$F-CMR, the more enlarged was EDV. Our data revealed threshold values: when the $^{19}$F-derived monocyte/macrophage signal exceeded 200 SNR × ml over the entire heart, it was associated with LV remodeling; when the border zone $^{19}$F SNR exceeded 8, it was associated with impaired remote myocardial wall thickening.

## Clinical perspectives and considerations

PFOB nanoemulsions have already been evaluated in clinical phase III studies as blood substitutes with similar application doses as used in the present study [35]. They are taken up by monocytes or macrophages irrespectively of their M1/M2 polarization in a time-dependent manner, while preserving their function [13, 26], which opens the translational perspective to develop $^{19}$F-based CMR imaging for future clinical applications. Due to the preferential uptake of PFOB nanoemulsions, $^{19}$F-based monocyte/macrophage imaging is rather cell-specific and directly quantifiable, as shown in the present study, and it might be even capable of being more specific when using functionalized nanoemulsions [11]. Intravenous administration of the nanoemulsion on day 3 after AMI enabled sufficient accumulation in monocytes/macrophages for sensitive detection by $^{19}$F-CMR within the infarcted myocardium on day 6 and was not associated with major side effects. Thus, $^{19}$F-CMR is capable to deliver in vivo information about early inflammatory infiltration after AMI. Inflammation can thus be visualized and followed as a potential additional target for subacute cardioprotection after AMI—beyond the already well established concept of preservation of coronary microcirculation [16].

Inflammation is a driver of adverse LV remodeling after AMI [44]. There are large inter-individual differences with respect to monocyte/macrophage quantity and localization in post-AMI inflammation [42]. The peri-infarct border zone, as identified by the specific gadolinium contrast agent uptake kinetics, is characterized by inflammatory infiltration, involved in the pathogenesis of arrhythmias [40] and associated with mortality [20].

For patients after AMI, it is currently unclear whether local hot spots of inflammation, a patchy pattern of inflammation in the infarct border, or the overall inflammatory volume in the heart drive clinical endpoints. The $^{19}$F platform might add novel information in this respect, since it specifically images monocytes/macrophages and thus can also monitor specific modulation of the inflammatory response by pharmacotherapy [21, 22, 28]. Compared to techniques using radiotracers, CMR is widely available and has better spatial resolution. In the future, the nanoemulsion delivery and the imaging workflow can easily be adopted to the management of patients after AMI in the hospital.

$^{1}$H CMR-derived tissue markers for improved prediction of cardiovascular endpoints are not always present after AMI. Major markers of mortality after AMI, such as MVO and IMH, appear in only 40% of all patients. The $^{19}$F signal will most probably be detectable in every singular individual myocardium post-AMI within the infarct region and border zone, thus enabling quantification of inflammatory patterns and extent. For patients after AMI, it is currently unclear whether local hot spots of inflammation, a patchy pattern of inflammation in the infarct border, or the overall inflammatory volume in the heart drive clinical endpoints. The $^{19}$F platform might add novel information in this respect, since it specifically images monocytes/macrophages and thus can also monitor specific modulation of the inflammatory response by pharmacotherapy [22]. However, whether or not these additional information further enhance the risk prediction after AMI needs to be tested in clinical trials.

## Study limitations

Since the present study aimed to mimic a clinical imaging scenario at day 6 with subsequent histological validation, the predictive value of the respective $^{1}$H- or $^{19}$F-derived signals on more long-term remodeling remains unclear. In mice, increased $^{19}$F-derived monocyte/macrophage signals predicted worsening of LV function also 28 days after AMI [3]. The time point of CMR analysis at 6 days post-AMI was chosen in line with recent expert consensus regarding the dynamic nature of infarct development and repair [19]. Our imaging study does not establish a cause-effect relationship between early inflammatory infiltration and impaired remote contractile function or LV remodeling early after reperfused AMI, but demonstrates a close association.

## Conclusion

In vivo $^{19}$F-CMR provides noninvasive visualization and quantification of monocytes/macrophages with reliable sensitivity and spatial resolution. In the present study using a pig model of reperfused AMI, in vivo $^{19}$F-CM identifed inflammatory infiltration as independent determinant of LV contractile function and geometry early after acute myocardial infarction. In a translational perspective, in vivo $^{19}$F-CMmight also enable loco-regional and longitudinal cell-specific CMR based imaging in AMI patients on a widely available technological platform. Thus, $^{19}$F-CMR, in addition to established $^{1}$H-based CMR, offers the potential to identify and characterize targets for novel anti-inflammatory therapeutic agents.

## Declarations

**Conflict of interest** The authors declare that they have nothing to disclose. The authors declare that they have no conflict of interest.

## References

1. Ambale-Venkatesh B, Yoneyama K, Sharma RK, Ohyama Y, Wu CO, Burke GL, Shea S, Gomes AS, Young AA, Bluemke DA, Lima JA (2017) Left ventricular shape predicts different types of cardiovascular events in the general population. Heart 103:499–507. https://doi.org/10.1136/heartjnl-2016-310052

2. Assimopoulos S, Shie N, Ramanan V, Qi X, Barry J, Strauss BH, Wright GA, Ghugre NR (2021) Hemorrhage promotes chronic adverse remodeling in acute myocardial infarction: a T1, T2 and BOLD study. NMR Biomed 34:e4404. https://doi.org/10.1002/nbm.4404

3. Bonner F, Jacoby C, Temme S, Borg N, Ding Z, Schrader J, Flogel U (2014) Multifunctional MR monitoring of the healing process after myocardial infarction. Basic Res Cardiol 109:430. https://doi.org/10.1007/s00395-014-0430-0

4. Bonner F, Merx MW, Klingel K, Begovatz P, Flogel U, Sager M, Temme S, Jacoby C, Salehi Ravesh M, Grapentin C, Schubert R, Bunke J, Roden M, Kelm M, Schrader J (2015) Monocyte imaging after myocardial infarction with 19F MRI at 3 T: a pilot study in explanted porcine hearts. Eur Heart J Cardiovasc Imaging 16:612–620. https://doi.org/10.1093/ehjci/jev008

5. Chowdhury MM, Tarkin JM, Albaghdadi MS, Evans NR, Le EPV, Berrett TB, Sadat U, Joshi FR, Warburton EA, Buscombe JR, Hayes PD, Dweck MR, Newby DE, Rudd JHF, Coughlin PA (2020) Vascular positron emission tomography and restenosis in symptomatic peripheral arterial disease: a prospective clinical study. JACC Cardiovasc Imaging 13:1008–1017. https://doi.org/10.1016/j.jcmg.2019.03.031

6. de Waha S, Patel MR, Granger CB, Ohman EM, Maehara A, Eitel I, Ben-Yehuda O, Jenkins P, Thiele H, Stone GW (2017) Relationship between microvascular obstruction and adverse events following primary percutaneous coronary intervention for ST-segment elevation myocardial infarction: an individual patient data pooled analysis from seven randomized trials. Eur Heart J 38:3502–3510. https://doi.org/10.1093/eurheartj/ehx414

7. Dorge H, Schulz R, Belosjorow S, Post H, van de Sand A, Konietzka I, Frede S, Hartung T, Vinten-Johansen J, Youker KA, Entman ML, Erbel R, Heusch G (2002) Coronary microembolization: the role of TNF-alpha in contractile dysfunction. J Mol Cell Cardiol 34:51–62. https://doi.org/10.1006/jmcc.2001.1489

8. Fernandez-Friera L, Fuster V, Lopez-Melgar B, Oliva B, Sanchez-Gonzalez J, Macias A, Perez-Asenjo B, Zamudio D, Alonso-Farto JC, Espana S, Mendiguren J, Bueno H, Garcia-Ruiz JM, Ibanez B, Fernandez-Ortiz A, Sanz J (2019) Vascular inflammation in subclinical atherosclerosis detected by hybrid PET/MRI. J Am Coll Cardiol 73:1371–1382. https://doi.org/10.1016/j.jacc.2018.12.075

9. Fernandez-Jimenez R, Galan-Arriola C, Sanchez-Gonzalez J, Aguero J, Lopez-Martin GJ, Gomez-Talavera S, Garcia-Prieto J, Benn A, Molina-Iracheta A, Barreiro-Perez M, Martin-Garcia A, Garcia-Lunar I, Pizarro G, Sanz J, Sanchez PL, Fuster V, Ibanez B (2017) Effect of ischemia duration and protective interventions on the temporal dynamics of tissue composition after myocardial infarction. Circ Res 121:439–450. https://doi.org/10.1161/CIRCRESAHA.117.310901

10. Flogel U, Ding Z, Hardung H, Jander S, Reichmann G, Jacoby C, Schubert R, Schrader J (2008) In vivo monitoring of inflammation after cardiac and cerebral ischemia by fluorine magnetic resonance imaging. Circulation 118:140–148. https://doi.org/10.1161/CIRCULATIONAHA.107.737890

11. Flogel U, Temme S, Jacoby C, Oerther T, Keul P, Flocke V, Wang X, Bonner F, Nienhaus F, Peter K, Schrader J, Grandoch M, Kelm M, Levkau B (2021) Multi-targeted (1)H/(19)F MRI unmasks specific danger patterns for emerging cardiovascular disorders. Nat Commun 12:5847. https://doi.org/10.1038/s41467-021-26146-6

12. Garcia-Prieto J, Villena-Gutierrez R, Gomez M, Bernardo E, Pun-Garcia A, Garcia-Lunar I, Crainiciuc G, Fernandez-Jimenez R, Sreeramkumar V, Bourio-Martinez R, Garcia-Ruiz JM, Del Valle AS, Sanz-Rosa D, Pizarro G, Fernandez-Ortiz A, Hidalgo A, Fuster V, Ibanez B (2017) Neutrophil stunning by metoprolol reduces infarct size. Nat Commun 8:14780. https://doi.org/10.1038/ncomms14780

13. Garello F, Boido M, Miglietti M, Bitonto V, Zenzola M, Filippi M, Arena F, Consolino L, Ghibaudi M, Terreno E (2021) Imaging of inflammation in spinal cord injury: novel insights on the usage of PFC-based contrast agents. Biomedicines. https://doi.org/10.3390/biomedicines9040379

14. Heimerl M, Sieve I, Ricke-Hoch M, Erschow S, Battmer K, Scherr M, Hilfiker-Kleiner D (2020) Neuraminidase-1 promotes heart failure after ischemia/reperfusion injury by affecting cardiomyocytes and invading monocytes/macrophages. Basic Res Cardiol 115:62. https://doi.org/10.1007/s00395-020-00821-z

15. Heusch G (2019) Coronary microvascular obstruction: the new frontier in cardioprotection. Basic Res Cardiol 114:45. https://doi.org/10.1007/s00395-019-0756-8

16. Heusch G (2020) Myocardial ischaemia-reperfusion injury and cardioprotection in perspective. Nat Rev Cardiol 17:773–789. https://doi.org/10.1038/s41569-020-0403-y

17. Heusch G (2021) Myocardial stunning and hibernation revisited. Nat Rev Cardiol 18:522–536. https://doi.org/10.1038/s41569-021-00506-7

18. Heusch G, Skyschally A, Schulz R (2011) The in-situ pig heart with regional ischemia/reperfusion - ready for translation. J Mol Cell Cardiol 50:951–963. https://doi.org/10.1016/j.yjmcc.2011.02.016

19. Ibanez B, Aletras AH, Arai AE, Arheden H, Bax J, Berry C, Bucciarelli-Ducci C, Croisille P, Dall'Armellina E, Dharmakumar R, Eitel I, Fernandez-Jimenez R, Friedrich MG, Garcia-Dorado D, Hausenloy DJ, Kim RJ, Kozerke S, Kramer CM, Salerno M,

Sanchez-Gonzalez J, Sanz J, Fuster V (2019) Cardiac MRI endpoints in myocardial infarction experimental and clinical trials: JACC scientific expert panel. J Am Coll Cardiol 74:238–256. https://doi.org/10.1016/j.jacc.2019.05.024

20. Jensch PJ, Stiermaier T, Reinstadler SJ, Feistritzer HJ, Desch S, Fuernau G, de Waha-Thiele S, Thiele H, Eitel I (2022) Prognostic relevance of peri-infarct zone measured by cardiovascular magnetic resonance in patients with ST-segment elevation myocardial infarction. Int J Cardiol 347:83–88. https://doi.org/10.1016/j.ijcard.2021.11.017

21. Jiao J, He S, Wang Y, Lu Y, Gu M, Li D, Tang T, Nie S, Zhang M, Lv B, Li J, Xia N, Cheng X (2021) Regulatory B cells improve ventricular remodeling after myocardial infarction by modulating monocyte migration. Basic Res Cardiol 116:46. https://doi.org/10.1007/s00395-021-00886-4

22. Klingenberg R, Stahli BE, Heg D, Denegri A, Manka R, Kapos I, von Eckardstein A, Carballo D, Hamm CW, Vietheer J, Rolf A, Landmesser U, Mach F, Moccetti T, Jung C, Kelm M, Munzel T, Pedrazzini G, Raber L, Windecker S, Matter CM, Ruschitzka F, Luscher TF (2022) Controlled-level EVERolimus in acute coronary syndrome (CLEVER-ACS)—a phase II, randomized, double-blind, multi-center, placebo-controlled trial. Am Heart J 247:33–41. https://doi.org/10.1016/j.ahj.2022.01.010

23. Lewis AJM, Miller JJ, Lau AZ, Curtis MK, Rider OJ, Choudhury RP, Neubauer S, Cunningham CH, Carr CA, Tyler DJ (2018) Non-invasive immunometabolic cardiac inflammation imaging using hyperpolarized magnetic resonance. Circ Res 122:1084–1093. https://doi.org/10.1161/CIRCRESAHA.117.312535

24. Nensa F, Poeppel T, Tezgah E, Heusch P, Nassenstein K, Mahabadi AA, Forsting M, Bockisch A, Erbel R, Heusch G, Schlosser T (2015) Integrated FDG PET/MR imaging for the assessment of myocardial salvage in reperfused acute myocardial infarction. Radiology 276:400–407. https://doi.org/10.1148/radiol.2015140564

25. Niccoli G, Montone RA, Ibanez B, Thiele H, Crea F, Heusch G, Bulluck H, Hausenloy DJ, Berry C, Stiermaier T, Camici PG, Eitel I (2019) Optimized treatment of ST-elevation myocardial infarction. Circ Res 125:245–258. https://doi.org/10.1161/CIRCRESAHA.119.315344

26. Nienhaus F, Colley D, Jahn A, Pfeiler S, Flocke V, Temme S, Kelm M, Gerdes N, Flogel U, Bonner F (2019) Phagocytosis of a PFOB-nanoemulsion for (19)F magnetic resonance imaging: first results in monocytes of patients with stable coronary artery disease and ST-elevation myocardial infarction. Molecules. https://doi.org/10.3390/molecules24112058

27. Pawlowsky K, Ernst L, Steitz J, Stopinski T, Kogel B, Henger A, Kluge R, Tolba R (2017) The Aachen Minipig: phenotype, genotype, hematological and biochemical characterization, and comparison to the Gottingen Minipig. Eur Surg Res 58:193–203. https://doi.org/10.1159/000471483

28. Pearce L, Davidson SM, Yellon DM (2021) Does remote ischaemic conditioning reduce inflammation? A focus on innate immunity and cytokine response. Basic Res Cardiol 116:12. https://doi.org/10.1007/s00395-021-00852-0

29. Reinstadler SJ, Stiermaier T, Reindl M, Feistritzer HJ, Fuernau G, Eitel C, Desch S, Klug G, Thiele H, Metzler B, Eitel I (2019) Intramyocardial haemorrhage and prognosis after ST-elevation myocardial infarction. Eur Heart J Cardiovasc Imaging 20:138–146. https://doi.org/10.1093/ehjci/jey101

30. Reiter T, Kircher M, Schirbel A, Werner RA, Kropf S, Ertl G, Buck AK, Wester HJ, Bauer WR, Lapa C (2018) Imaging of C-X-C motif chemokine receptor CXCR4 expression after myocardial infarction with [(68)Ga]Pentixafor-PET/CT in correlation with cardiac MRI. JACC Cardiovasc Imaging 11:1541–1543. https://doi.org/10.1016/j.jcmg.2018.01.001

31. Rischpler C, Dirschinger RJ, Nekolla SG, Kossmann H, Nicolosi S, Hanus F, van Marwick S, Kunze KP, Meinicke A, Gotze K, Kastrati A, Langwieser N, Ibrahim T, Nahrendorf M, Schwaiger M, Laugwitz KL (2016) Prospective evaluation of 18F-fluorodeoxyglucose uptake in postischemic myocardium by simultaneous positron emission tomography/magnetic resonance imaging as a prognostic marker of functional outcome. Circ Cardiovasc Imaging 9:e004316. https://doi.org/10.1161/CIRCIMAGING.115.004316

32. Rischpler C, Nekolla SG, Heusch G, Umutlu L, Rassaf T, Heusch P, Herrmann K, Nensa F (2019) Cardiac PET/MRI-an update. Eur J Hybrid Imaging 3:2. https://doi.org/10.1186/s41824-018-0050-2

33. Rothe M, Jahn A, Weiss K, Hwang JH, Szendroedi J, Kelm M, Schrader J, Roden M, Flogel U, Bonner F (2019) In vivo (19)F MR inflammation imaging after myocardial infarction in a large animal model at 3 T. MAGMA 32:5–13. https://doi.org/10.1007/s10334-018-0714-8

34. Schulz-Menger J, Bluemke DA, Bremerich J, Flamm SD, Fogel MA, Friedrich MG, Kim RJ, von Knobelsdorff-Brenkenhoff F, Kramer CM, Pennell DJ, Plein S, Nagel E (2020) Standardized image interpretation and post-processing in cardiovascular magnetic resonance—2020 update: Society for Cardiovascular Magnetic Resonance (SCMR): Board of Trustees Task Force on Standardized Post-Processing. J Cardiovasc Magn Reson 22:19. https://doi.org/10.1186/s12968-020-00610-6

35. Spahn DR, Waschke KF, Standl T, Motsch J, Van Huynegem L, Welte M, Gombotz H, Coriat P, Verkh L, Faithfull S, Keipert P, European Perflubron Emulsion in Non-Cardiac Surgery Study G (2002) Use of perflubron emulsion to decrease allogeneic blood transfusion in high-blood-loss non-cardiac surgery: results of a European phase 3 study. Anesthesiology 97:1338–1349. https://doi.org/10.1097/00000542-200212000-00004

36. Stone GW, Selker HP, Thiele H, Patel MR, Udelson JE, Ohman EM, Maehara A, Eitel I, Granger CB, Jenkins PL, Nichols M, Ben-Yehuda O (2016) Relationship between infarct size and outcomes following primary PCI: patient-level analysis from 10 randomized trials. J Am Coll Cardiol 67:1674–1683. https://doi.org/10.1016/j.jacc.2016.01.069

37. Swirski FK, Nahrendorf M (2018) Cardioimmunology: the immune system in cardiac homeostasis and disease. Nat Rev Immunol 18:733–744. https://doi.org/10.1038/s41577-018-0065-8

38. Tardif JC, Kouz S, Waters DD, Bertrand OF, Diaz R, Maggioni AP, Pinto FJ, Ibrahim R, Gamra H, Kiwan GS, Berry C, Lopez-Sendon J, Ostadal P, Koenig W, Angoulvant D, Gregoire JC, Lavoie MA, Dube MP, Rhainds D, Provencher M, Blondeau L, Orfanos A, L'Allier PL, Guertin MC, Roubille F (2019) Efficacy and safety of low-dose colchicine after myocardial infarction. N Engl J Med 381:2497–2505. https://doi.org/10.1056/NEJMoa1912388

39. Tarkin JM, Calcagno C, Dweck MR, Evans NR, Chowdhury MM, Gopalan D, Newby DE, Fayad ZA, Bennett MR, Rudd JHF (2019) (68)Ga-DOTATATE PET identifies residual myocardial inflammation and bone marrow activation after myocardial infarction. J Am Coll Cardiol 73:2489–2491. https://doi.org/10.1016/j.jacc.2019.02.052

40. Tulumen E, Rudic B, Ringlage H, Hohneck A, Roger S, Liebe V, Kuschyk J, Overhoff D, Budjan J, Akin I, Borggrefe M, Papavassiliu T (2021) Extent of peri-infarct scar on late gadolinium enhancement cardiac magnetic resonance imaging and outcome in patients with ischemic cardiomyopathy. Heart Rhythm 18:954–961. https://doi.org/10.1016/j.hrthm.2021.01.023

41. van der Bijl P, Abou R, Goedemans L, Gersh BJ, Holmes DR Jr, Ajmone Marsan N, Delgado V, Bax JJ (2020) Left ventricular post-infarct remodeling: implications for systolic function improvement and outcomes in the modern era. JACC Heart Fail 8:131–140. https://doi.org/10.1016/j.jchf.2019.08.014

42. van der Laan AM, Ter Horst EN, Delewi R, Begieneman MP, Krijnen PA, Hirsch A, Lavaei M, Nahrendorf M, Horrevoets AJ,

Niessen HW, Piek JJ (2014) Monocyte subset accumulation in the human heart following acute myocardial infarction and the role of the spleen as monocyte reservoir. Eur Heart J 35:376–385. https://doi.org/10.1093/eurheartj/eht331

43. Virani SS, Alonso A, Aparicio HJ, Benjamin EJ, Bittencourt MS, Callaway CW, Carson AP, Chamberlain AM, Cheng S, Delling FN, Elkind MSV, Evenson KR, Ferguson JF, Gupta DK, Khan SS, Kissela BM, Knutson KL, Lee CD, Lewis TT, Liu J, Loop MS, Lutsey PL, Ma J, Mackey J, Martin SS, Matchar DB, Mussolino ME, Navaneethan SD, Perak AM, Roth GA, Samad Z, Satou GM, Schroeder EB, Shah SH, Shay CM, Stokes A, VanWagner LB, Wang NY, Tsao CW, American Heart Association Council on E, Prevention Statistics C, Stroke Statistics S (2021) Heart disease and stroke statistics-2021 update: a report from the American Heart Association. Circulation 143:e254–e743. https://doi.org/10.1161/CIR.0000000000000950

44. Westman PC, Lipinski MJ, Luger D, Waksman R, Bonow RO, Wu E, Epstein SE (2016) Inflammation as a driver of adverse left ventricular remodeling after acute myocardial infarction. J Am Coll Cardiol 67:2050–2060. https://doi.org/10.1016/j.jacc.2016.01.073

45. Ye YX, Basse-Lusebrink TC, Arias-Loza PA, Kocoski V, Kampf T, Gan Q, Bauer E, Sparka S, Helluy X, Hu K, Hiller KH, Boivin-Jahns V, Jakob PM, Jahns R, Bauer WR (2013) Monitoring of monocyte recruitment in reperfused myocardial infarction with intramyocardial hemorrhage and microvascular obstruction by combined fluorine 19 and proton cardiac magnetic resonance imaging. Circulation 128:1878–1888. https://doi.org/10.1161/CIRCULATIONAHA.113.000731

46. Yilmaz A, Dengler MA, van der Kuip H, Yildiz H, Rosch S, Klumpp S, Klingel K, Kandolf R, Helluy X, Hiller KH, Jakob PM, Sechtem U (2013) Imaging of myocardial infarction using ultrasmall superparamagnetic iron oxide nanoparticles: a human study using a multiparametric cardiovascular magnetic resonance imaging approach. Eur Heart J 34:462–475. https://doi.org/10.1093/eurheartj/ehs366

## Authors and Affiliations

**Florian Bönner[1]** · **M. Gastl[1]** · **F. Nienhaus[1]** · **M. Rothe[2,3]** · **A. Jahn[1,4]** · **S. Pfeiler[1]** · **U. Gross[5]** · **H.-P. Schultheiss[5]** · **B. Ibanez[6,7,8]** · **S. Kozerke[9]** · **J. Szendroedi[10]** · **M. Roden[2,3,10]** · **R. Westenfeld[1]** · **J. Schrader[11,12]** · **U. Flögel[11,14]** · **G. Heusch[13]** · **M. Kelm[1,14]**

1   Division of Cardiology, Pulmonology, and Vascular Medicine, Medical Faculty Heinrich Heine University, Moorenstr. 5, 40225 Düsseldorf, Germany

2   Institute for Clinical Diabetology, German Diabetes Center, Leibniz Center for Diabetes Research, Düsseldorf, Germany

3   German Center for Diabetes Research, Partner, Düsseldorf, Germany

4   Central Animal Research Facility, Heinrich Heine University, Düsseldorf, Germany

5   Institute for Cardiac Diagnostics and Therapy (IKDT), Berlin, Germany

6   Centro Nacional de Investigaciones Cardiovasculares Carlos III (CNIC), Madrid, Spain

7   IIS-Fundación Jiménez Díaz Hospital, Madrid, Spain

8   CIBERCV, Madrid, Spain

9   Institute for Biomedical Engineering, University and ETH Zurich, Zurich, Switzerland

10  Division of Endocrinology and Diabetology, Medical Faculty, Heinrich Heine University, Düsseldorf, Germany

11  Department of Molecular Cardiology, Heinrich Heine University, Düsseldorf, Germany

12  Experimental Cardiovascular Imaging, Department of Molecular Cardiology, Heinrich Heine University, Düsseldorf, Germany

13  Institute for Pathophysiology, West German Heart and Vascular Center, University of Essen Medical School, Essen, Germany

14  Cardiovascular Research Institute Düsseldorf (CARID), Medical Faculty, Heinrich Heine University, Düsseldorf, Germany